

## VECTOR IMAGING OF MAGNETIC MICROSTRUCTURE

M. H. Kelley, John Unguris, M. R. Scheinfein,  
D. T. Pierce, and R. J. Celotta

An ability to study the properties of microscopic magnetic structures and to investigate magnetic properties with submicron spatial resolution is important both for its fundamental scientific value and its usefulness in applied magnetic technology. As the size of magnetic devices decreases, and the density of recorded information increases, new diagnostic techniques must be developed with which these new magnetic structures and processing techniques can be characterized. Many current techniques for the investigation of magnetic structures suffer either from poor spatial resolution or from the inability clearly to separate contrast due to magnetic structures from that due to topographic or other physical features. We describe a method of magnetic imaging that overcomes many of the difficulties of other current techniques and that allows quantitative analysis at high spatial resolution of the vectorial properties of sample magnetization.

### *Experimental Method*

Magnetization arises from the orientation of the magnetic moments of individual electrons in bulk material. Consequently, the problem of microscopic characterization of magnetic properties can be resolved by measurement of the spin orientation of electrons in a small region of a magnetic solid. The technique described in this work is based on the observation that low-energy secondary electrons produced by high-energy electron bombardment, as in scanning electron microscopy (SEM), retain the spin orientation they had in the bulk.<sup>1</sup> A measurement of the spin polarization of these secondary electrons gives a direct measurement of the magnetization in the small region from which the secondary electrons originate (Fig. 1). The technique of imaging magnetic microstructure through spin analysis of electrons ejected by a focused high-energy electron beam has been called Scanning Electron Microscopy with Polarization Analysis (SEMPA).<sup>2-4</sup>

The SEMPA technique has several features that make it an attractive tool for micromagnetic studies. First, the spatial resolution is substantially better than for any other currently available technique for studying bulk specimens. The resolution in SEMPA is the same as in conventional SEM images, with a potential resolution better than 10 nm. Sec-

ond, unlike other methods used to study magnetic microstructure, the magnetic information from SEMPA is essentially independent of, but recorded simultaneously with, the topographic information. This separation makes possible detailed studies of the relationship between physical and magnetic structures. Third, the polarization signal and magnetic contrast are large. The secondary-electron current can typically be 10-50% of the incident electron beam, and typically has a spin polarization between 5% and 30%, depending on the sample. Finally, SEMPA is a surface analytical tool because the secondary electrons have a mean escape depth of only a few nanometers. SEMPA is thus an excellent tool for studies of the magnetic properties of surfaces and thin films.

Our SEMPA apparatus (Fig. 2) has three basic components: the electron microscope, the secondary-electron collection and transport optics, and the spin polarimeter.<sup>5,8</sup> The SEM is fully ultrahigh-vacuum compatible and is fitted with an ion gun for surface cleaning and an Auger analyzer for surface characterization. A spatial resolution of 40 nm can be achieved with this instrument. The electron optics collect the spin-polarized secondaries emitted from the sample and form them into a beam suitable for use with the spin polarization analyzers.

The two spin analyzers together allow for the determination of all three orthogonal components of the vector magnetization. The first detector, referred to as in-plane in Fig. 2, measures two components,  $P_x$  and  $P_y$ , in the plane of the sample surface. The second detector, referred to as out-of-plane in Fig. 2, is oriented perpendicular to the in-plane detector and measures both the out-of-plane component  $P_z$  and a redundant in-plane component, which provides a diagnostic for the calibration of the two spin analyzers. An electrostatic quarter-spherical switchyard determines which of the two SEMPA detectors is active.

The basis for spin analysis is the scattering of a spin-polarized electron from an atom with large nuclear charge, gold in this case. There is a relativistic effect, the spin-orbit interaction, which causes spin-polarized electrons to be scattered with different probability into two detectors that are symmetrically placed relative to the direction of incidence. This scattering asymmetry is used in spin analyzers to determine the polarization of an incident electron beam.

Our spin analyzer consists of an annular anode that is split into four quadrants, each of which measures the intensity of electrons backscattered from an evaporated gold film and

---

The authors are at the Center for Atomic, Molecular, and Optical Physics, National Institute of Standards and Technology, Gaithersburg, MD 20899. This work supported in part by the Office of Naval Research.

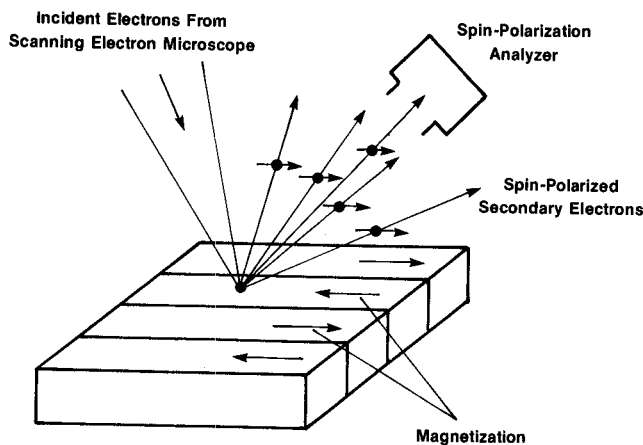
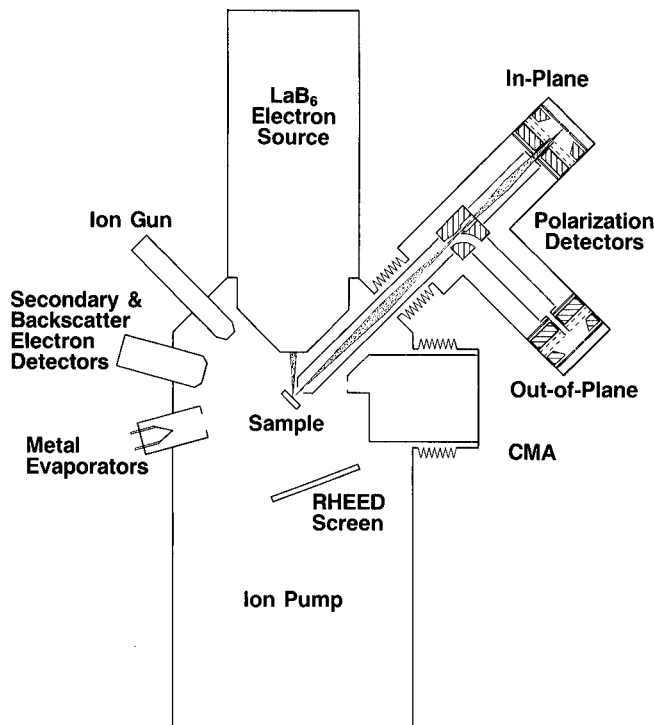


FIG. 1.--Principle of scanning electron microscopy with polarization analysis (SEMPA).  
 FIG. 2.--Schematic of SEMPA apparatus.



amplified by a microchannel plate multiplier. A pair of opposed quadrants determines one component of the incident spin polarization, say  $P_x$ , through the relationship:

$$P_x = \frac{1}{S} \frac{I_a - I_b}{I_a + I_b} \quad (1)$$

where  $I_a$  and  $I_b$  are the electron fluxes measured by the two quadrants, and  $S$  is the analyzing power of the detector. Each SEMPA detector determines two orthogonal components of the spin polarization, and hence of the sample magnetization. The sum of the intensities from any two opposing quadrants is proportional to the total secondary-electron current. As the primary electron beam is rastered over the sample, each detector *simultaneously* measures the conventional secondary-electron image and two images giving the electron spin polarization projected along two perpendicular axes.

A single crystal iron whisker provides a good system for illustrating the SEMPA technique. The magnetic properties of iron single crystals are quite well understood, so the interpretation of the polarization images is straightforward. In particular, for the case of an iron (100) surface, the magnetization is parallel to the surface along one of the two easy magnetization axes. Because there is no out-of-plane component, only data from the in-plane detector are necessary. In addition, the magnitude of the magnetization in ferromagnetic materials is constant and does not depend on the direction. Figure 3 shows both the conventional secondary-electron image and the  $P_x$  and  $P_y$  polarization components for a small region of the whisker. Several features of these images are particularly noteworthy. First, contrast between the magnetic domains is clearly visible in the polarization images, magnetization in the positive  $x$  or  $y$  direction (or spin polarization is the negative  $x$  or  $y$  direction) is indicated by white pixels. The second important feature is the presence of two instrument effects that interfere with accurate polarization measurements. One effect

allows a remnant of the topographic image to be visible in both  $P_x$  and  $P_y$ . The other contributes a background polarization signal that varies smoothly over the images. Both these experimental artifacts must be corrected by the data analysis. Finally, in the format in which the data are presented in Fig. 3, it is rather difficult to visualize or to interpret quantitatively what is going on in the magnetic structure.

There are thus two areas of immediate interest: (1) what data processing is required to permit quantitative analysis of the polarization images, and (2) how the results should be presented for the most convenient interpretation.

#### Raw Data Processing

Data processing is required to minimize two basic problems: spurious feedthrough of topographical information into the polarization images, and systematic offsets for zero polarization. Each is caused by a lack of azimuthal symmetry about the detector axis as the electron beam strikes the gold target. Any physical asymmetry causes an artificial asymmetry between the signals collected by opposing pairs of anode quadrants and results in artificial polarization contrast. For example, as the primary electron beam is scanned over the sample, the secondary electron beam may be scanned over the gold target. This feature gives rise to the smoothly varying background in the polarization images. Topographic features appear in the polarization images because the secondary electrons from a surface with topographical structure are not emitted with azimuthal symmetry about the mean surface normal. These systematic effects can be minimized, but not always completely eliminated, by careful adjustment of the secondary electron transport optics. One final instrumental effect, the

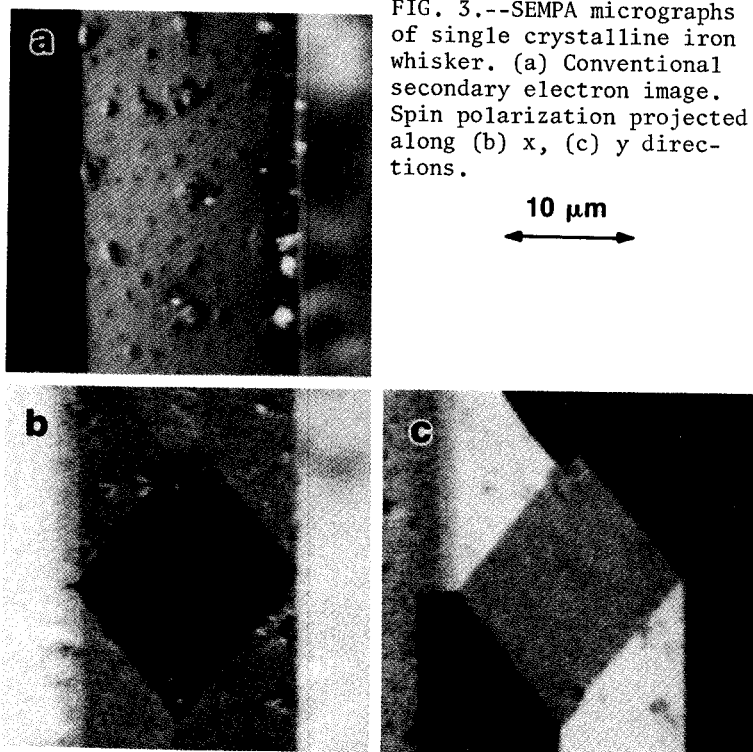


FIG. 3.--SEMPA micrographs of single crystalline iron whisker. (a) Conventional secondary electron image. Spin polarization projected along (b) x, (c) y directions.

overall detection efficiency of individual quadrants, adds a polarization offset that is constant over an entire image.

In practice, one can determine the artificial polarizations very reliably by recording for each image a corresponding image in which the magnetic information is absent, by replacing the gold target in the detector by a graphite target. Carbon atoms have insufficient nuclear charge to generate polarization contrast through the spin-orbit interaction, so that the graphite-scattered images contain only the systematic and artificial asymmetries and can be used to correct the polarization data, apart from the constant overall zero offset.

Graphite background images for the previously shown region of the iron whisker are presented in Fig. 4. The extraneous topographic features are clearly visible. Figure 5 shows the images with the graphite backgrounds subtracted. The smoothly varying background has been removed, along with much of the ex-

traneous structure. The remaining small features are likely real, the result of nonmagnetic contamination of this sample.

There are two principal concerns about the background correction process. First, the noise in the corrected images has increased by roughly  $\sqrt{2}$  because the noise in both primary images contributes to the difference image. Second, because the gold-scattered and graphite-scattered images are recorded separately, small drifts in the apparatus can introduce registration problems between the two images. The registration can be adjusted with the image processing software and has so far presented no major difficulties.

At this point, the polarization information is essentially correct as displayed. The remaining problem is that neither the gold-scattered images nor the graphite background images have a well-defined absolute zero of polarization. If the two images have different zero offsets, that difference will appear in the corrected images as well. For the iron whisker images, the correction is straightforward because one has prior knowledge that the magnitude of the polarization is constant across the image. A bias polarization can be determined and subtracted from each image such that the resultant image has maximally uniform polarization magnitude.

For samples where such prior knowledge is not available, the zero bias must be determined in some other manner. Our preferred technique is to record test images of nonmagnetic samples, using both the gold and graphic scattering targets. On the basis of these nonmagnetic data, fine adjustments to the transport optics and detector gains can be made so that the zero bias for the gold-scattered and graphite-scattered images is the same. That done, subtraction of the graphite background also corrects for the zero bias.

#### Presentation of Results

Thus far, the magnetic information has been presented in terms of the projections of the spin polarization along three orthogonal axes. Because visualization of vector fields is generally difficult, an alternate representation is desirable in which the most important features are clearly emphasized. For the magnetic domains in an iron whisker, and many similar systems, there are two important goals. The first is to determine the direction of the magnetization vector in order to study the relative orientation of adjacent domains. The second is to study the magnitude uniformity of the magnetization independent of its direction. For such studies, it is convenient to present images that correspond to the magnitude and direction of the in-plane spin polarization. These images, referred to as  $Q_{xy}$  and  $D_{xy}$ , respectively, are related to  $P_x$  and  $P_y$  by

$$Q_{xy} = \sqrt{P_x^2 + P_y^2}$$

$$(2) \quad D_{xy} = \tan^{-1} \frac{P_x}{P_y} \quad (3)$$

These images for the iron whisker are shown in Fig. 6. It is evident in Fig. 6(a) that the magnitude is essentially constant, with the possible exception of the domain walls where there

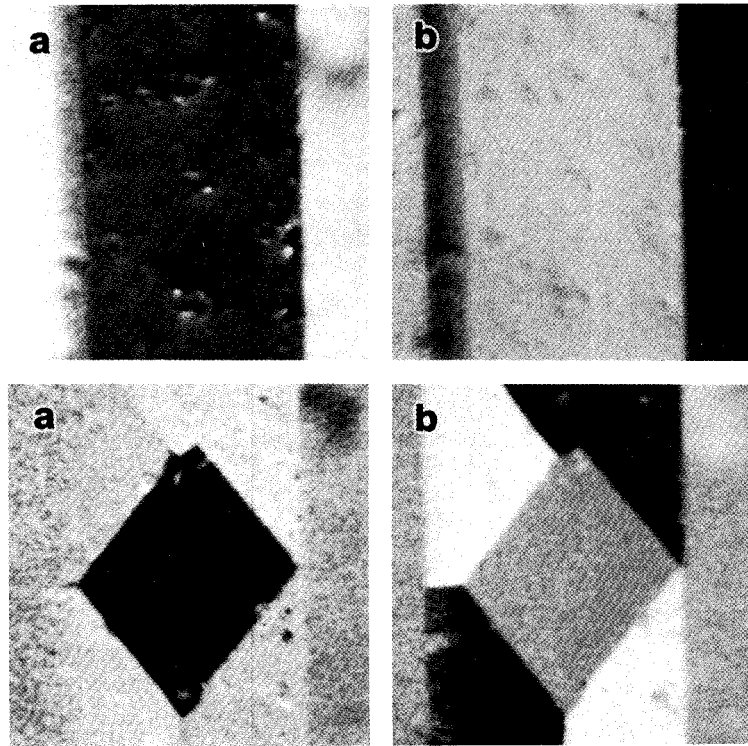


FIG. 4.--Iron whisker. Instrument induced polarization contrast along (a) x, (b) y directions.  
 FIG. 5.--Iron whisker. (a) x, (b) y components of spin polarization, corrected for instrumental effects.

4 is an apparent drop in polarization. The detailed behavior of magnetization in domain walls is an important topic, but the spatial resolution of the present images is insufficient for quantitative analysis of the walls. One principal effect of finite resolution on the determination of a signed quantity like the spin polarization is to depress the apparent magnitude in regions, such as the domain walls, where the sign changes rapidly. This finite resolution effect can fully account for the deficit observed in Fig. 6(a).

5 In Fig. 6(b) the in-plane spin polarization direction is shown. Dark corresponds to polarization in the +x direction, with increasing angles (in the counterclockwise sense) represented by increasing intensity in the image, until white again corresponds to the +x direction. Arrows in the figure indicate the mean polarization direction for the several domains. The polarization direction can be determined quite well with this technique. A pixel intensity histogram for Fig. 6(b) indicates an approximately Gaussian distribution of angles with a width of about  $\pm 10^\circ$  about the mean polarization direction. The width of the mean is indicative of the extent to which the uniformity of spin polarization throughout a domain

can be verified. The angular difference between the mean polarization directions for adjacent domains can be determined substantially more accurately.

This representation, which is convenient for the two in-plane components, becomes almost essential for the visualization of the vector field in systems where out-of-plane magnetization is also possible. An example of such a system with large out-of-plane magnetization is cobalt. The crystal orientation of the cobalt sample studied was such that the preferred magnetization direction for the bulk was normal to the surface. In order to reduce the magnetic energy at the surface, the magnetic domains break up at the surface in a complex way, but retain a significant out-of-plane component to the magnetization. The in-plane component is constrained by crystal anisotropies to lie primarily along the six crystalline symmetry axes. Images of  $P_x$ ,  $P_y$ , and  $P_z$  for the cobalt samples are shown in Fig. 7. The observed vector field is rather complex and difficult to deduce from inspection of these images; the need for a more convenient representation is clearly indicated. As in the previously discussed case of magnetization in iron, the important physical questions concern the uniformity of the in-plane and total polarization magnitudes, the in-plane direction, and the component out-of-plane of the total polarization vector.

In Fig. 8 are shown the images for the in-plane direction and magnitude. Six intensity levels, corresponding to regions polarized primarily along each of the six crystalline axes, are clearly visible in Fig. 8(b). It is also apparent that a gray scale is not the best representation for the angular information. Whenever possible (as in the oral presentation of this work) color can be used to significant advantage for representing the direction information.

The apparent deficit at the domain walls of the in-plane polarization magnitude is very pronounced in Fig. 8(a), and significantly larger than that expected from a consideration of finite resolution effects. This finding seems to indicate a real loss of the in-plane spin polarization at the domain walls. It can be seen from Fig. 7(c) that the in-plane domain walls correspond very well with regions of large positive or large negative out-of-plane polarization.

The picture that emerges from inspection of Figs. 7(c) and 8 is that at domain walls, where the in-plane components of the magnetic vectors from the adjacent domains point toward each other, the composite magnetization is directed into the sample. Where the adjacent in-plane vectors point away from each other, the net magnetization points out of the sample. It is as if underlying bulk domains, which are polarized normal to the surface, act as "sources" or "sinks" of the observed polarization vectors. Further measurements will be required to characterize the magnetic properties of this sample fully.

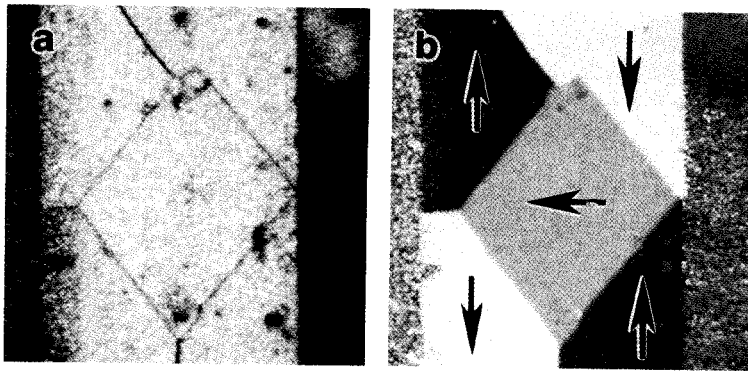
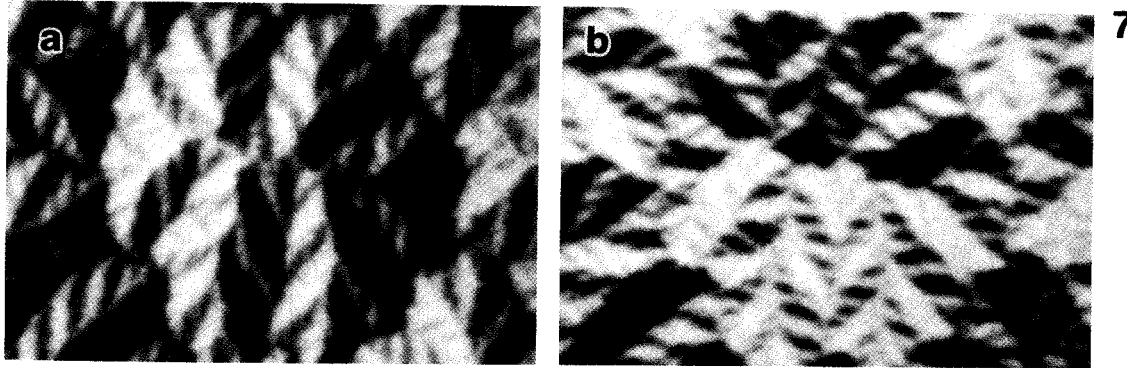
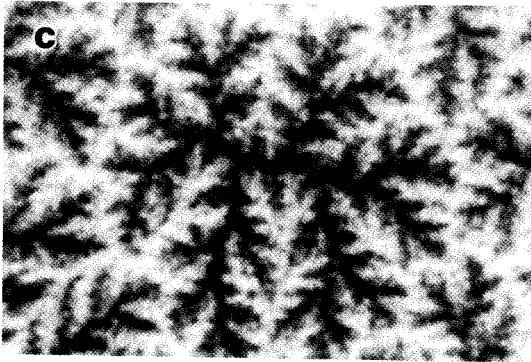


FIG. 6.--Iron whisker. (a) Magnitude, (b) direction of in-plane polarization.



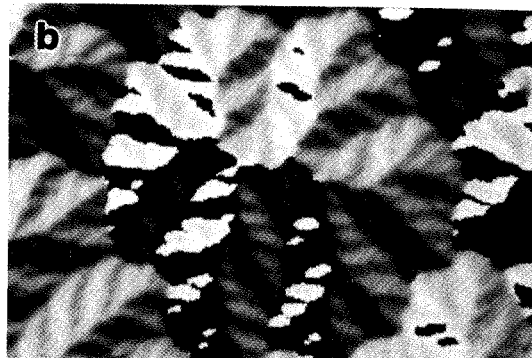
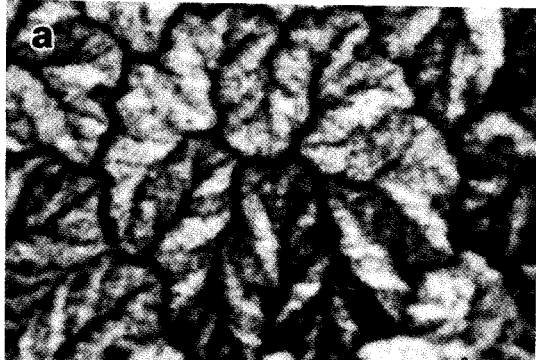
7



5.0  $\mu\text{m}$

FIG. 7.--SEMPA micrographs for cobalt single crystal. Projections of spin polarization along (a) x, (b) y, (c) z directions.

FIG. 8.--Cobalt single crystal. (a) Magnitude, (b) direction of in-plane polarization.



8

### Conclusions

It has been shown in the present work that with adequate data-processing techniques, quantitative studies of vector magnetic properties can be performed. It has further been demonstrated that a judicious choice of data representation can aid enormously in the visualization of the magnetic vector fields.

### References

1. D. R. Penn and S. P. Apell, *Phys. Rev. B* 32: 7753, 1985.
2. G. G. Hembree, J. Unguris, R. J. Gelotta,

and D. T. Pierce, *Scanning Microscopy Suppl.* 1: 229, 1987.

3. K. Koike, H. Matsuyama, and K. Hayakawa, *ibid.*, p. 241.

4. R. J. Gelotta and D. T. Pierce, *Science* 234: 249, 1986.

5. J. Unguris, D. T. Pierce, and R. J. Gelotta, *Rev. Sci. Instrum.* 57: 1314, 1986.

6. M. R. Scheinfein, D. T. Pierce, J. Unguris, J. J. McClelland, R. J. Gelotta, and M. H. Kelley, *ibid.*, 60: 1, 1989.

7. J. Kessler, *Polarized Electrons*, Berlin: Springer, 1985.